Percolation and diffusion in three-component lipid bilayers: effect of cholesterol on an equimolar mixture of two phosphatidylcholines

Paulo F. F. Almeida,* Winchil L. C. Vaz,‡ and T. E. Thompson*

*Department of Biochemistry, University of Virginia School of Medicine, Charlottesville, Virginia 22908 USA; and ‡Max-Planck-Institut für Biophysikalische Chemie, Postfach 2841, DW-3400 Göttingen, Germany

ABSTRACT The lateral diffusion of a phospholipid probe is studied in bilayers of binary mixtures of dimyristoylphosphatidylcholine (DMPC)/cholesterol and distearoylphosphatidylcholine (DSPC)/cholesterol and in the ternary system DMPC/DSPC/cholesterol using fluorescence recovery after photobleaching. An approximate phase diagram for the ternary system, as a function of temperature and cholesterol concentration, was obtained using differential scanning calorimetry and the phase diagrams of the binary systems. This phase diagram is similar to those of the phospholipid/cholesterol binary mixtures. In bilayers where solid and liquid phases coexist, the diffusion results are interpreted in terms of phase percolation. The size of the liquid-phase domains is estimated using percolation theory. In the ternary system, addition of cholesterol up to ~20 mol% shifts the percolation threshold to lower area fractions of liquid, but the size of the liquid-phase domains does not change. Above ~20 mol% cholesterol, the liquid phase is always connected. The size of solid-phase domain clusters is estimated using a model recently developed (Almeida, P. F. F., W. L. C. Vaz, and T. E. Thompson. 1992. *Biochemistry.* 31:7198–7210). For cholesterol concentrations up to 20 mol%, the size of solid-phase domain units does not change. Beyond 20 mol%, cholesterol causes the size of the solid units to decrease.

INTRODUCTION

If the components of a lipid bilayer form a nonideal mixture, solid and liquid-crystalline phases can coexist in the plane of the bilayer, over a large temperature interval, at a constant pressure (1, 2). Consider a mixed bilayer completely in the liquid phase, the stable state at high temperatures. When the temperature is decreased, the system enters the two-phase, solid-liquid coexistence region. Initially, the liquid phase is completely continuous, and the solid phase is composed of isolated domains. Eventually, at a low enough temperature, the system contains just enough liquid so that the liquid is still continuous. At this point, a small decrease in temperature will reverse the connectivity of the two phases: the liquid phase becomes disconnected and the solid phase becomes continuous throughout the plane of the bilayer. This point is the percolation threshold, p_c (3, 4).

Many molecules, including some membrane proteins and lipid species with low melting temperatures, are essentially insoluble in solid phases. Therefore, below the percolation threshold, their diffusion is confined to small isolated liquid-phase domains. Whether the percolation threshold plays a role in regulation of biological membrane processes is not known. However, the possibility exists that it constitutes a mechanism the cell may use to control the activity of membrane proteins (5).

Vaz et al. (6) showed how the technique of fluorescence recovery after photobleaching (FRAP)[1] can be used to determine the percolation threshold in phospholipid systems by studying the binary mixture dimyristoylphosphatidylcholine (DMPC)/distearoylphosphatidylcholine (DSPC). Since then, several systems have been studied with this method (7–9). The percolation threshold depends strongly on the system, and some of the features that determine how much liquid exists at that point are beginning to be apparent. Since cholesterol is a major component of mammalian plasma membranes, it is of fundamental importance to know how it affects the percolation threshold in phospholipid mixtures.

Diffusion in DMPC/cholesterol mixtures above the melting temperature (T_m) of the phospholipid has been investigated previously (10). The corresponding study below T_m in DMPC/cholesterol and in DSPC/cholesterol is now reported. The investigation of these binary systems is necessary for the understanding of the ternary system but is also interesting on its own merit. Recently, detailed phase diagrams of phospholipid/cholesterol binary mixtures have become available. The theoretical work of Ipsen et al. (11, 12) on the dipalmitoylphosphatidylcholine (DPPC)/cholesterol system supported the basic features of the phase diagrams determined by electron spin resonance (ESR) by Shimshick and McConnell (13), which indicated that the phosphatidylcholine/cholesterol mixtures constitute monotectic systems. The most salient characteristic of this type of system is the existence of a liquid–liquid miscibility gap (14). This was corroborated by differential scanning calorimetry (DSC) (15) and ESR studies (16, 17). The definition of the different two-phase regions in the phase diagram has

Address correspondence to T. E. Thompson.

The present address of Paulo F. F. Almeida and Winchil L. C. Vaz is Unidade de Ciências Exactas e Humanas, Universidade do Algarve, Campus de Gambelas, P-8000 Faro, Portugal.

[1] *Abbreviations used in this paper:* DMPC, dimyristoylphosphatidylcholine; DPPC, dipalmitoylphosphatidylcholine; DSC, differential scanning calorimetry; DSPC, distearoylphosphatidylcholine; ESR, electron spin resonance; FRAP, fluorescence recovery after photobleaching; NBD-C(12)-PE, *N*-(7-nitrobenzoxa-2,3-diazol-4-yl)-didodecanoylphosphatidylethanolamine.

0006-3495/93/02/399/14 $2.00

thus become very precise. Above the T_m of the phospholipid, a two-phase region exists where liquid-ordered (l_o) and liquid-disordered (l_d) phases coexist; below the T_m, a two-phase region exists where solid and l_o phases coexist. In the l_d phase, which exists at low cholesterol concentrations, the cholesterol molecules are thought to span both monolayers of the phospholipid bilayer. In the l_o phase, which exists at high cholesterol concentration, the cholesterol molecules are thought to be packed in a manner analogous to the phospholipids, spanning only one monolayer (17, 18). Because of the higher cholesterol concentration in the l_o phase, the total area per phospholipid is larger there than in the l_d phase.

Recent improvement in the FRAP apparatus and data analysis (6) allowed us to attempt a critical evaluation of two models that have been proposed to explain the observations of Rubenstein et al. (19) on phospholipid diffusion in DMPC/cholesterol mixtures. One model (20) invokes a phase boundary as the reason for an abrupt change in the diffusion coefficient at a well-defined temperature and composition. The other attributes these results to the system crossing the percolation threshold (21, 22). We find that the latter explanation is more likely to be correct.

A first approximation to the phase diagram of DMPC/DSPC/cholesterol is constructed partially from DSC and from the phase diagrams of the three binary mixtures of each possible pair of components. The essential features of the thermodynamic behavior of the ternary system appear to be a consequence of a differential partitioning of cholesterol between regions rich in DMPC and regions rich in DSPC.

The effect of cholesterol on the percolation properties of a DMPC/DSPC equimolar mixture is also examined. In this ternary system, addition of cholesterol causes a shift of the percolation threshold to lower fractions of liquid phase; eventually, above ~20 mol% cholesterol the liquid is always continuous. Cholesterol has little effect on the size of the liquid and solid domains. The results are in good agreement with percolation theory.

MATERIALS AND METHODS

DMPC and DSPC were purchased from Avanti Polar Lipids, Inc. (Alabaster, AL). Cholesterol was obtained from Serva Fine Biochemicals (Heidelberg, Germany). The high purity of the lipids was confirmed by thin-layer chromatography. All lipids were used without further purification. Chloroform solutions of the lipids were prepared and stored at −20°C. The NBD-C(10)′ and -C(12)′ probes were prepared as described before (23).

FRAP experiments

A detailed description of the FRAP experiments was provided in our recent publications (6, 9, 10). In this study, we use identical methods and present here only a brief outline of them. The samples studied were flat stacks of a few hundred water-separated bilayers. The NBD probe was incorporated in phospholipid/cholesterol mixtures at a probe to lipid molar ratio of 1:1,000. *N*-(7-nitrobenzoxa-2,3-diazol-4-yl)didecanoylphosphatidylethanolamine was used in DMPC/cholesterol binary mixtures, and *N*-(7-nitrobenzoxa-2,3-diazol-4-yl)-di dodecanoylphosphatidylethanolamine (NBD-C(12)-PE) was used in DSPC/cholesterol and in DSPC/DMPC/cholesterol mixtures. Both probes partition exclusively into the liquid phase when the chain length of the probe is significantly shorter than the chain length of the host lipid (difference ≥ 4 carbons, approximately; Vaz, W. L. C., unpublished observations). However, when the solid phase is composed of DMPC only, this condition might not obtain if NBD-C(12)-PE were used. The FRAP measurements were performed using a uniform circular beam profile with a radius of 2.5–4.0 μm. To make possible comparison between different experiments, all values of the recovery time τ reported here are normalized to a bleach spot radius of 3 μm, unless otherwise indicated. The measurements were begun at 58°C. The samples were cooled by setting the control unit to a desired temperature and waiting for a period of ≥30 min before each measurement. When the temperature was changed by >2°C, this was done in steps of 2°C, waiting for ~10 min between each change. Only cooling scans were performed, because in previous studies either no hysteresis was observed (6) or the cooling scan represented the equilibrium curve (9). The recovery curves were fitted to the theoretical equations of Soumpasis (24) using the Simplex algorithm (Quantum Chemistry Exchange Program, J. P. Chandler, Oklahoma State University, Stillwater, OK). Allowance was made for the existence of more than one recovery component by using a linear ramp for the possible slow components.

Calorimetry

Multibilayer vesicles in excess water were prepared by mixing the components together in chloroform and evaporating the solvent in a rotary evaporator at 60°C. The lipid was hydrated at ~95°C with 10 mM *N*-2-hydroxyethylpiperazine-*N*′-2-ethane sulfonic acid buffer, pH 7.6 (at 20°C), 50 mM KCl, 1 mM ethylenediaminetetraacetate, 0.02% NaN_3, to a final concentration of ~100 mM in phospholipid. The dispersions were stirred for a short period at the same temperature, rapidly cooled to 70°C, and then cooled at <5°C/h to room temperature and incubated for ~24 h. The heat capacity curves were obtained by DSC with a calorimeter modified to allow scanning at a constant rate, as in previous work (9). The scan rate was 10°C/h in the heating mode. The DSC scans were corrected for the thermal response of the calorimeter. The enthalpies associated with the transition were calculated from the integrated heat capacity curves and the concentration of phospholipid, determined by phosphate assay (25).

Fractional areas of liquid and solid phases in DMPC/DSPC/cholesterol

A knowledge of the area fractions of coexisting liquid and solid phases is essential for a discussion of the results in terms of percolation theory. The total liquid ($l_o + l_d$) area fraction can be obtained from the heat capacity curves with a few simple assumptions.

First, we assume that the decrease in ΔH for the transitions in DPPC/cholesterol mixtures (26) is due to formation of l_o phase—a certain amount of phospholipid does not then undergo melting. This is equivalent to considering a partitioning of the total ΔH,

$$\Delta H_{total} = \Delta H_{solid-l_o} + \Delta H_{l_o-l_d}. \quad (1)$$

Using the phase diagram of DPPC/cholesterol (17) to calculate the fractions of the phases coexisting at each cholesterol concentration and the calorimetric data of Estep et al. (26), we estimate that the enthalpy change associated with the $l_o - l_d$ transition is ~30% (per mole of phospholipid) of that associated with the pure DPPC solid $- l_d$ transition. In conjunction with Eq. 1, this implies

$$\Delta H_{solid-l_o} \simeq \Delta H_{total}/1.3. \quad (2)$$

Second, we assume that the area per phospholipid molecule is ~45 Å^2 in the solid (27), 60 Å^2 in the l_d, and 80 Å^2 in the l_o phase (10).

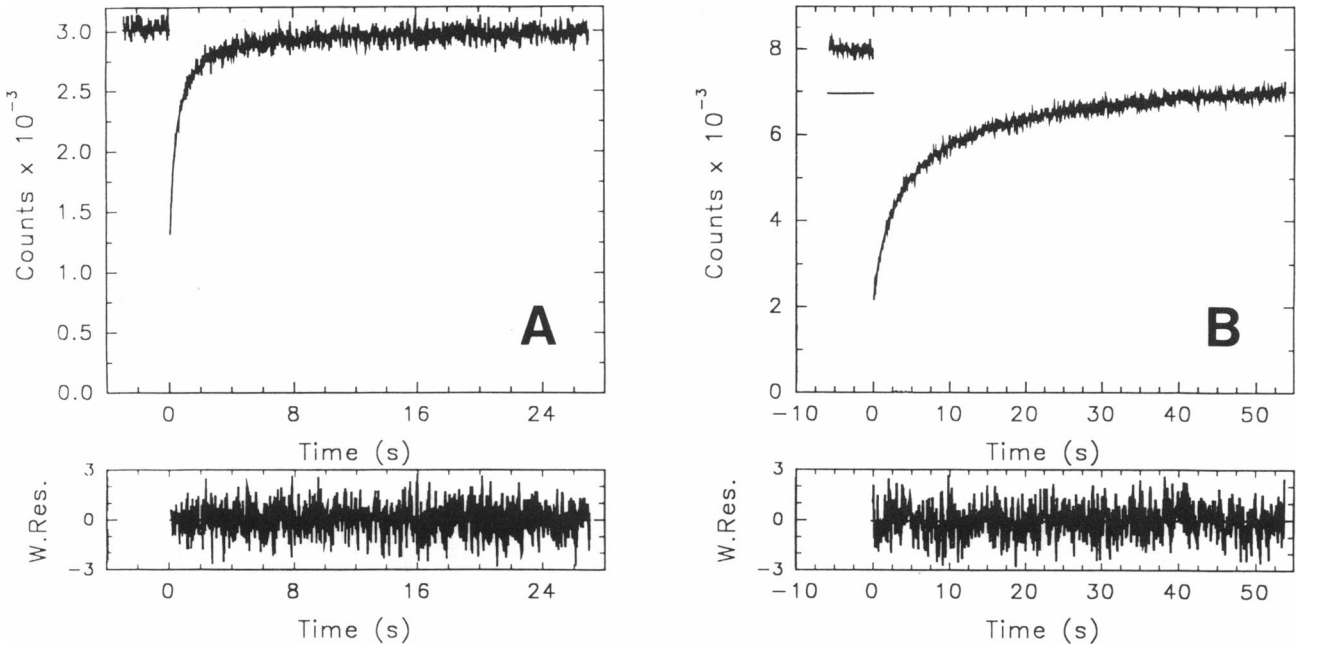

FIGURE 1 Typical FRAP curves in DMPC/cholesterol 75:25 above and below the line of connectivity. The upper panel shows the fluorescence recovery and the bottom panel shows the weighted residuals in units of standard deviations. The line on the right side of the upper panels indicates the fluorescence intensity at infinite time. (*A*) 48°C, fit parameters are τ = 0.304 s, recovery = 99.0%, slope = 0.0 counts/s, χ^2 = 1.1; (*B*) 14°C, τ = 3.07 s, recovery = 85.6%, slope = 6.5 counts/s, χ^2 = 1.0. The values of τ given are not normalized.

These areas are only weakly temperature-dependent, so the error made by using a constant value is small.

The mass fraction of the total liquid phase is obtained as a function of temperature from the integral of the heat capacity curves of Fig. 4 and from the assumption of the partitioning of the total ΔH (Eqs. 1 and 2). The consequences for diffusion and percolation would be qualitatively identical if the factor of 1.3 in Eq. 2 were slightly different, e.g., 1.2. The numerical values of the solid-phase obstacle radius and of the percolation threshold, p_c, obtained below would then differ a little, but all values would change in the same direction.

In the mixtures containing 0 or 4 mol% cholesterol, it is evident that half of the transition is completed at ~36°C; the DSPC-rich transition has a larger ΔH simply because the ΔH of the phase transition of pure DSPC is larger than that of pure DMPC (2). Therefore, in these two mixtures, the liquid mass fractions were calculated from the integral of the heat capacity using two appropriate weighing factors, different before and after 36°C. In the other mixtures, although the heat capacity curves are not symmetrical, the correction gained from a subdivision would be small, and there is no simple and reasonable way of splitting the transitions.

RESULTS

We present first the results obtained in the solid $-l_o$ coexistence region in DMPC/cholesterol and DSPC/cholesterol and then the results obtained in the ternary system formed from these components.

Binary systems DMPC/cholesterol and DSPC/cholesterol

FRAP experiments

Two typical fluorescence recovery curves are shown in Fig. 1, obtained in DMPC/cholesterol 75:25 (mol/mol) at 48°C (*A*) and 14°C (*B*). At this latter temperature, it is clear that recovery is incomplete. Incomplete recoveries are consistently observed in a defined interval of temperatures and compositions. This is shown in Fig. 2 for three concentrations of cholesterol (15, 20, and 25 mol%) in DSPC/cholesterol (*A–C*) and DMPC/cholesterol (*D–F*). The behavior of the recovery time τ ($\tau = \omega^2/4D$, where ω is the spot radius and D the diffusion coefficient) as a function of temperature is also presented in this figure.

As the temperature is decreased, the recovery is essentially complete up to a well-defined point and then drops continuously (Fig. 2). This break point has been operationally defined as the point of liquid-phase connectivity (6, 7), but because it may differ somewhat from the percolation threshold p_c (for reasons that will become apparent when we discuss the ternary system) we will refer to it as $p_{100\%}$.

The recovery time reaches a local maximum at the percolation threshold in some systems (9). In the phase diagrams of DMPC/cholesterol and DSPC/cholesterol (Fig. 3), the lines defined by $p_{100\%}$ (●, *A* and *B*) and the maxima or inflections of τ (○, *B*) are presented.

We could not obtain the complete curves of the percent recovery as a function of temperature (Fig. 2) because of water condensation on the sample slide below 10°C (in DMPC/cholesterol) or because τ became extremely long at the lower temperatures and the laser was not stable throughout these periods (in DSPC/choles-

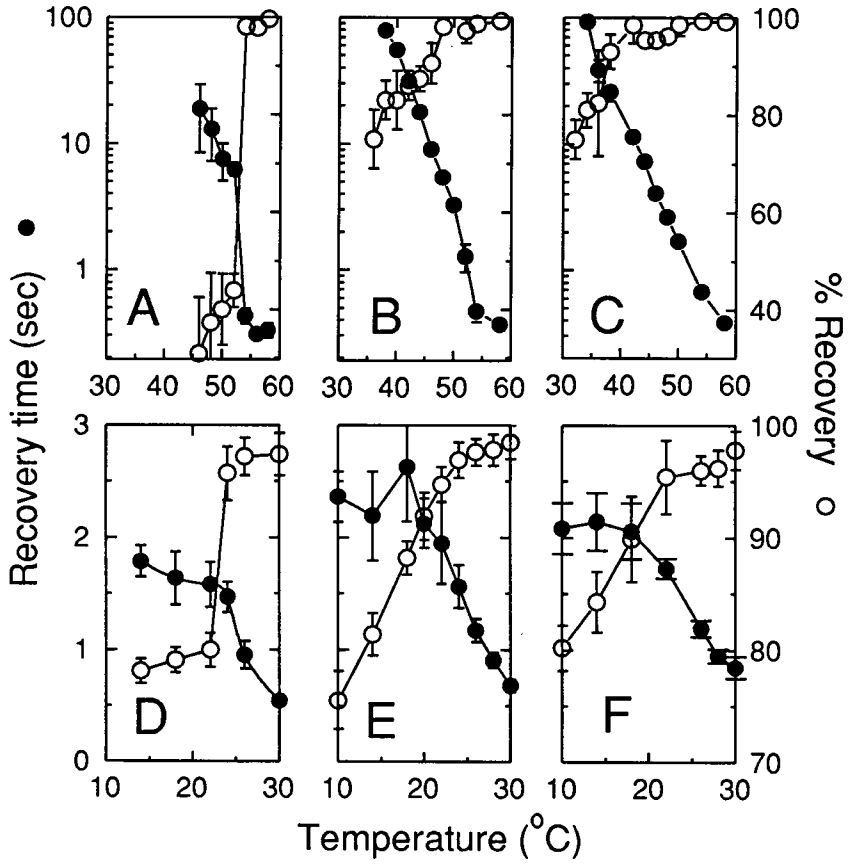

FIGURE 2 Recovery time and percent recovery as a function of temperature in DSPC/cholesterol 85:15 (*A*), 80:20 (*B*), 75:25 (*C*), and in DMPC/cholesterol 85:15 (*D*), 80:20 (*E*), 75:25 (*F*). All values of τ are normalized to a spot radius of 3 μm. Notice that the scale of τ is logarithmic in DSPC/cholesterol. Each point represents an average of eight measurements in two independent samples (in DMPC/cholesterol) or four measurements in the same sample (in DSPC/cholesterol); the error bars are the corresponding standard deviations (most are buried inside the points in DSPC/cholesterol).

terol). Therefore, it was not possible to define clearly the percolation threshold p_c for these two systems.

Ternary system DMPC/DSPC/cholesterol

Calorimetry

The heat capacity curves are shown in Fig. 4, for DMPC/DSPC 1:1 mixtures containing various concentrations of cholesterol (0, 4, 7, 10, 15, 18, 20, 25, and 35 mol%). In DMPC/DSPC 1:1 the transition clearly has two maxima. The low-temperature maximum corresponds to melting of DMPC-rich regions and the high-temperature maximum corresponds to melting of DSPC-rich regions. The partition coefficient of cholesterol between these two types of regions must be different from 1, because addition of only 4 mol% cholesterol causes a dramatic decrease of the heat capacity peak associated with the DMPC-rich the transition but hardly changes the DSPC-rich transition (a similar argument was given by Demel et al. [28]).

The total enthalpy change ΔH associated with the transition is plotted in Fig. 5 as a function of cholesterol concentration. There is an initial drop, but then ΔH remains almost constant until 20 mol% cholesterol, after which it again decreases.

FRAP experiments

The percent recovery and the recovery time were measured by FRAP in DMPC/DSPC 1:1 mixtures containing various concentrations of cholesterol (0, 4, 7, 10, 15, 18, 20, 25, and 35 mol%) as a function of temperature. The results are shown in Fig. 6. In some of the curves, the recovery appears to increase below the percolation threshold as the temperature is decreased. This is probably an artifact of the fitting process. We tried to obtain from the fit the fastest component of τ only (diffusion in the liquid phase), but this proved to be difficult in some cases because other components of τ were not sufficiently slow compared with the fastest component. The result is that the slower components also contribute to τ given by the fit. As these slower components correspond to larger recoveries, the fit gives a larger percent recovery. However, if we compare the fluorescence recovery after a given time t in each FRAP curve, then we find

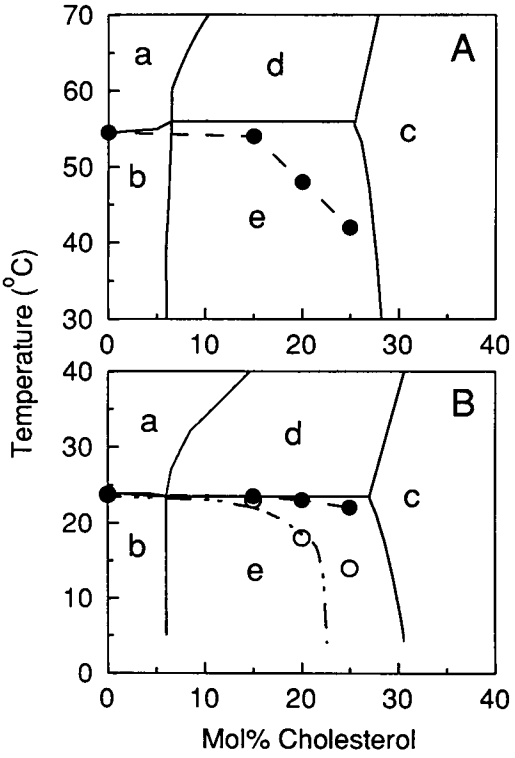

FIGURE 3 Phase diagrams of (*A*) DSPC/cholesterol and (*B*) DMPC/cholesterol obtained with ESR spectroscopy (Sankaram, M. B., and T. E. Thompson, unpublished observations); the lines were drawn following our best judgement through the data points (not shown). A more complete version of the DMPC/cholesterol phase diagram has been published in our previous work (10). The phases present in the regions identified are as follows: *a*, l_d; *b*, solid; *c*, l_o; *d*, $l_o + l_d$; *e*, solid + l_o. The $p_{100\%}$ points (●) and the maxima/inflections of τ (○) are indicated. The dash-dot line (*B*) is from Rubenstein et al. (19).

that recovery at t either decreases or remains constant as the temperature decreases. Probably, the only way of clearly deciding this problem would require making a multicomponent fit to the recovery curves. We have not done so.

Phase diagram and line of connectivity

The onset and completion temperatures (defined by 1 and 99% melting from the integrated heat capacity curves) and the peak temperatures for each transition are indicated in Fig. 7.

The percolation thresholds of the liquid phase in each mixture are indicated by the arrows above the corresponding heat capacity curve (Fig. 4) and by the filled circles in the phase diagram (Fig. 7). It will be described in the Discussion how the percolation thresholds are obtained, but they essentially coincide with the temperature at which the percent recovery shows an abrupt change (Fig. 6).

The percolation point for DMPC/DSPC 1:1 cannot be determined with the method used for the cholesterol containing mixtures (see Discussion) and is therefore not indicated. However, the location of the line of connectivity is similar to that in the phospholipid/cholesterol binary mixtures; assuming that the line of connectivity at low cholesterol concentrations is similar in the binary and in the ternary mixtures, we can extrapolate the initial portion of this line to zero cholesterol in the ternary system and obtain the percolation threshold in the DMPC/DSPC 1:1 binary mixture at 39°C. The measured $p_{100\%}$ point (6) in this mixture is ~43°C.

The calorimetric results can be understood if cholesterol partitions differentially into regions richer in DMPC or DSPC. Consider a hypothetical system comprised of two subsystems in thermal equilibrium but separated from each other by a barrier impermeable to all lipids. Each subsystem is a "binary" mixture of cholesterol with one of the two solids coexisting in DMPC/DSPC 1:1 below the phase transition region (29, 30).

Now, all mixtures of saturated phospholipids with cholesterol studied so far give rise to similar phase diagrams (Fig. 3) (16, 17), where the monotectic horizontal approximately coincides, in each case, with the T_m of the phospholipid. Thus, we expect that both hypothetical

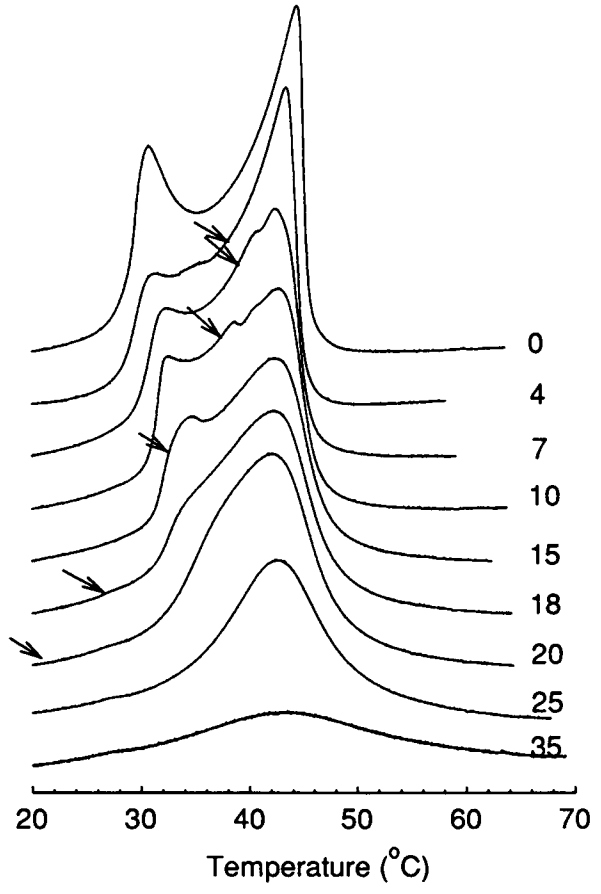

FIGURE 4 Excess heat capacity curves in DMPC/DSPC 1:1 containing the mol% cholesterol indicated on the right side of each curve: from top to bottom, 0, 4, 7, 10, 15, 18, 20, 25, and 35 mol% cholesterol. The arrows mark the percolation thresholds determined by FRAP.

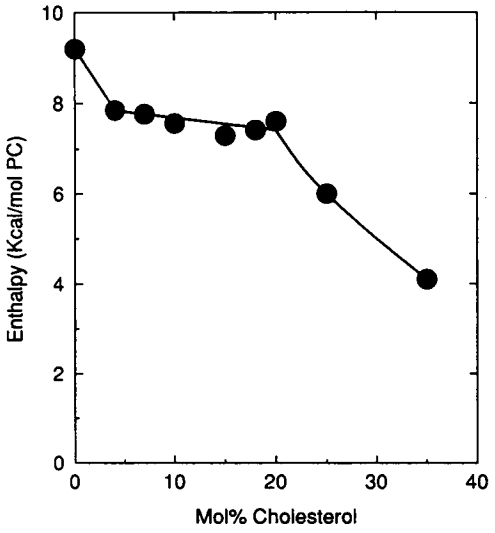

FIGURE 5 Total enthalpy of the transition per mole of phospholipid as a function of cholesterol concentration. The line reflects our interpretation of the data.

subsystems under consideration (DMPC-rich/cholesterol and DSPC-rich/cholesterol) would show identical behavior. The monotectic horizontal would now essentially match the maxima in the excess heat capacity curves in DMPC/DSPC 1:1 (Fig. 4; uppermost excess heat capacity curve).

What happens if the original barrier is replaced by one that is still impermeable to phospholipid but permeable to cholesterol? When equilibrium is attained, the cholesterol concentration in the subsystem richer in DMPC is higher because cholesterol prefers DMPC-rich regions. Assuming a cholesterol partition coefficient of 2 in favor of the DMPC-rich areas, we can calculate a first order approximation to the phase diagram of the ternary system, regarded as a union of the two binary subsystems. The result is shown in Fig. 7 (*dashed lines*). Plotted against the global cholesterol concentration, the phase diagram of the DMPC-rich/cholesterol subsystem shrinks and shifts to the left because the cholesterol concentration in DMPC-rich regions is higher than the global cholesterol concentration. The phase diagram of the DSPC-rich/cholesterol subsystem broadens and shifts to the right because the effective cholesterol concentration in DSPC-rich regions is lower than the global cholesterol concentration. Using a partitioning coefficient of 3 would produce a very similar result—the major effect is obtained when its value is changed from 1 to 2. The coexistence region in the ternary system—defined by the outer lines of the overlapping phase diagrams—extends over a broader range of temperatures and cholesterol concentrations than in the binary mixtures. By analogy to the phase diagrams of the binary mixtures of DMPC/cholesterol and DSPC/cholesterol (Fig. 3), it is possible to identify the regions where solid, l_d, and l_o phases may be present. However, some evidence exists from ESR (Sankaram, M. B., and T. E. Thompson, unpublished observations) that the phase diagram of the ternary system is simpler than a union of the two diagrams; in some of the areas of the phase diagram where the three phases, solid, l_o, and l_d, could coexist, only solid and l_o appear to be present. Also, at 4 mol% cholesterol, the heat capacity curve already shows a shoulder on the DMPC-rich transition that is characteristic of the presence of l_o phase. Therefore, the solidus boundary must be located at lower cholesterol compositions than indicated. This means that at low cholesterol concentrations the partition coefficient of cholesterol must be even >2 in favor of DMPC-rich regions.

The heat capacity maximum associated with the DMPC-rich transition moves to higher temperatures as the cholesterol concentration increases. This is explained if the l_o phase formed from the DMPC-rich solid is yet richer in DMPC: the solid becomes poorer in its lower-melting component and its T_m rises. The temperature of the peak of the DSPC-rich transition decreases initially and then remains constant. The initial decrease could arise because of the differential partitioning of cholesterol between solid and liquid phases.

The behavior of the total enthalpy change ΔH associated with the solid-liquid transition in the ternary system contrasts with the strictly monotonic decrease in ΔH observed in DPPC/cholesterol (26). Again, the observations can be explained by the differential partitioning of cholesterol between solid and l_o phases and between DMPC-rich and DSPC-rich regions. On addition of small amounts of cholesterol to a DMPC/DSPC mixture, an l_o phase appears that is enriched in DMPC relative to DSPC. Cholesterol prefers the l_o phase to the solid phase; the phase boundaries (Fig. 3) show that the solid contains ~6 mol%, whereas the l_o phase contains ~30 mol% cholesterol. Thus, additional cholesterol will go preferentially into the preformed l_o phase. In a sense, this phase acts as a buffer that prevents use of the DSPC-rich solid to make l_o phase. Although the DSPC-rich solid is not significantly used, the total ΔH does not decrease much because the DSPC-rich transition contributes most to it. This is consistent with the approximate phase diagram we propose (Fig. 7): up to 22.5 mol% cholesterol the l_o phase can grow at the expense of DMPC-rich solid. Above that concentration, there is no more of this solid to be used, the DSPC-rich solid begins to be significantly consumed, and the total ΔH decreases (Fig. 5).

In conclusion, the approximate phase diagram for the ternary system is consistent with the experimental data presented. The phase behavior of the ternary mixture is determined by three facts: (*a*) in DMPC/DSPC 1:1, two immiscible solids coexist below the onset temperature of the transition; (*b*) cholesterol partitions preferentially into liquid phases when solid and liquid coexist; and (*c*)

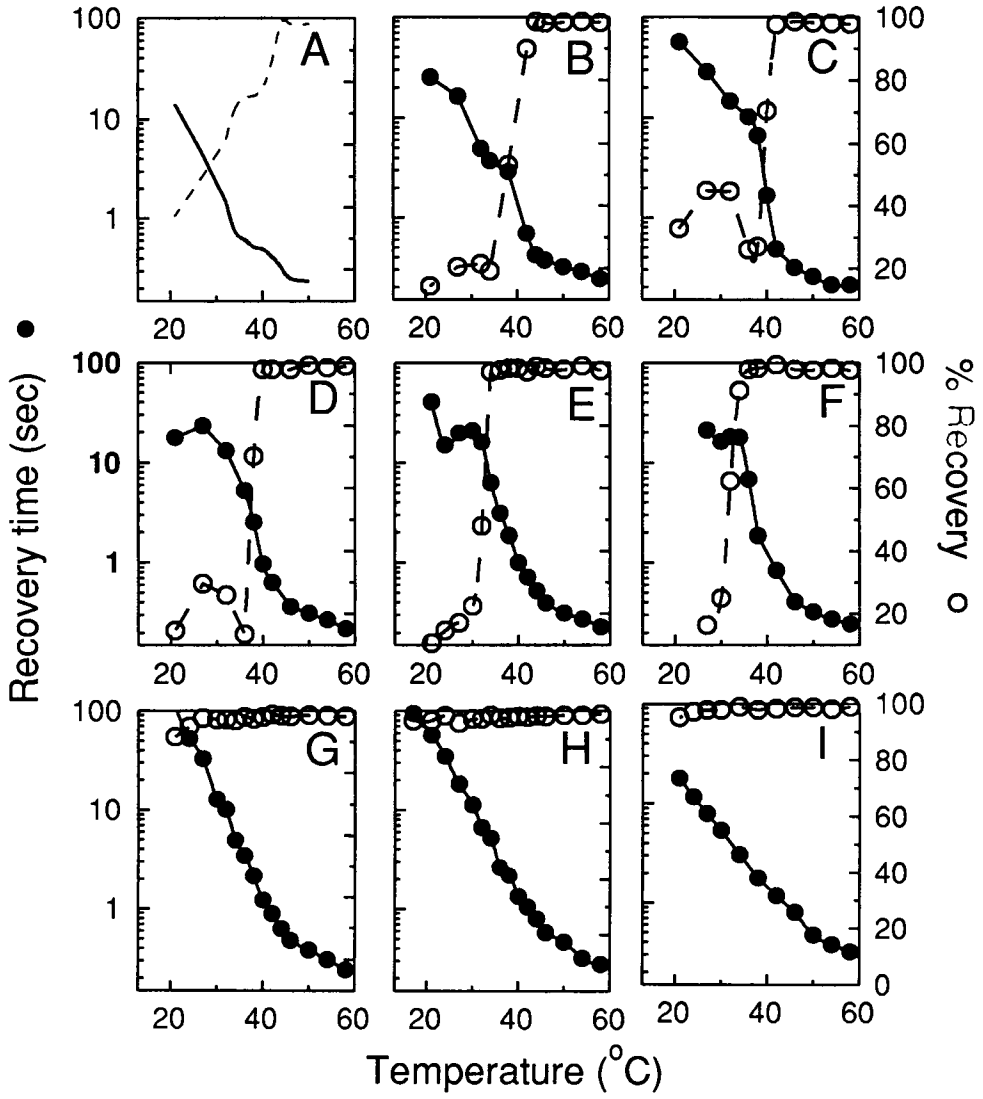

FIGURE 6 Recovery time τ (●, *solid line*) and percent recovery (○, *dashed line*) as a function of temperature in DMPC/DSPC 1:1 containing the following cholesterol concentrations: 0 mol% (*A*), 4 mol% (*B*), 7 mol% (*C*), 10 mol% (*D*), 15 mol% (*E*), 18 mol% (*F*), 20 mol% (*G*), 25 mol% (*H*), and 35 mol% (*I*). The lines in *A* (0 mol%) are from the cooling scan in Vaz et al. (6). Each data point represents the average of eight measurements in two independent samples. Error bars are not indicated for the sake of clarity. They are shown in Fig. 10 for the percent recovery. The standard deviations on the values of τ are typically of 10%, above the percolation threshold; at or below that point, they range between ~20 and 100%.

cholesterol partitions preferentially into regions richer in DMPC.

DISCUSSION

Binary systems DMPC/cholesterol and DSPC/cholesterol

FRAP experiments

Using periodic pattern photobleaching, Rubenstein et al. (19) observed an abrupt increase in the diffusion coefficient of a NBD-PE probe, between 20 and 25 mol% cholesterol, below T_m of the phospholipid. Owicki and McConnell (20) explained the abrupt increase in diffusion by the disappearance of a solid phase formed by parallel ridges of almost pure phospholipid. Diffusion across these ridges would be slow, and their disappearance would therefore cause an increase in the diffusion coefficient of a lipid molecule. At the temperature at which the ridges disappear and if the ridges are much longer than the radius of the bleached spot in our FRAP experiments, this model predicts the observation of a dramatic change in the diffusion coefficient, whereas the recovery should still be complete and arising from a single diffusing component. (Diffusion across the ridges being extremely slow [a few orders of magnitude slower than in the "valleys"], long range diffusion in the system

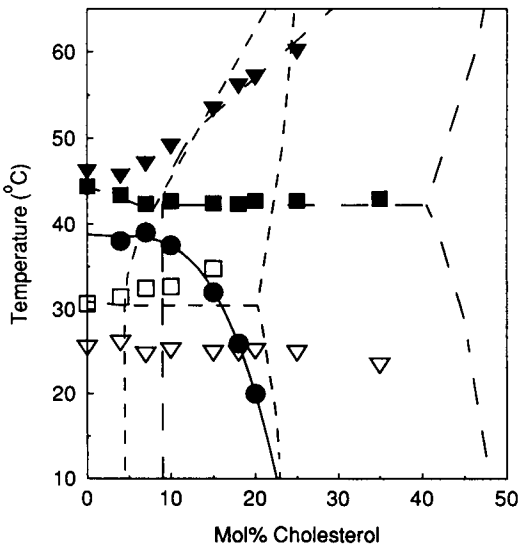

FIGURE 7 Qualitative phase diagram for DMPC/DSPC 1:1 as a function of cholesterol concentration and temperature. Indicated are the onset (▽) and completion (▼) temperatures of the transition, the heat capacity peaks at low (□) and high temperatures (■), and the percolation points (●). The solid line is the line of connectivity. See text for the meaning of dashed lines.

would become essentially a one-dimensional process, occurring only in the valleys in the direction of the ridges.)

An alternative explanation proposed for the observations of Rubenstein et al. (19) is that the system reaches the percolation threshold for the liquid phase when the cholesterol concentration is increased beyond a critical value (21, 22); the liquid phase becomes continuous and diffusion becomes faster.

Snyder and Freire (21) treated the lipid bilayer as a triangular lattice where each site is occupied by a phospholipid. The cholesterol molecules intercalate between two phospholipids. At high cholesterol concentrations, intercalation of dimers of cholesterol may occur. The nearest-neighbor interaction energy is adjusted to give the best fit to the total enthalpy of the transition determined by calorimetry. Depending on the magnitude of this interaction, the size of cholesterol-rich domains will vary. The pair-connectedness function of the cholesterol-rich regions shows an abrupt increase from ~0 to 1 at ~20 mol% cholesterol.

Slater and Caille (22) also considered a lattice model to represent the lipid bilayer. Here, each site is occupied by a phospholipid molecule in one of three possible states: solid, liquid, or in a 3.5:1 phospholipid:cholesterol complex. Notice the close correspondence between these states and the solid, l_d, and l_o phases. The authors arrive at conclusions very similar to those of Snyder and Freire (21), with a percolation threshold for the 3.5:1 complex state at ~20 mol% cholesterol.

According to the percolation model, the change in the diffusion coefficient at the percolation threshold may be small, but a significant change in the percent recovery must occur. The observation of incomplete recoveries agrees with the percolation model but not with the solid-phase ridge model if the length of the ridges is much larger than the diameter of the bleached spot. Rubenstein et al. (19) obtained the diffusion coefficients from a linear regression of the logarithm of the fluorescence amplitude and did not consider the possibility of fractional recovery. In a periodic pattern photobleaching experiment (the technique they used), the fluorescence rises back to only half the prebleach intensity, resulting in a smaller signal-to-noise ratio than in the spot photobleaching method we use. Therefore, if the recovery was ~80% in their experiments as it is in ours, it would probably be difficult to distinguish it from complete recovery.

The lines defined by the $p_{100\%}$ and the maxima in τ are approximations to the line of connectivity, which divides the phase diagram in two regions: above it or to its right, the liquid phase is continuous, and below it, the liquid phase is disconnected by the solid. The maxima or inflections in τ in DMPC/cholesterol fall close to the line drawn by Rubenstein et al. (19), dividing the phase diagram into regions of slow and fast diffusion (*dash-dot line* in Fig. 3 *B*).

Ternary system DMPC/DSPC/cholesterol

The FRAP and DSC data are used together to arrive at some conclusions about the properties of liquid and solid phases in this system. Information about the solid phase can be obtained from the diffusion coefficient and about the liquid phase from the limiting recovery.

It is convenient to define some terms that will be used frequently. To facilitate reference to the literature on percolation, we designate the fractional area of the liquid phase by p and that of the solid phase by c. Accordingly, p_c is the percolation threshold for the liquid phase and c_p is the percolation threshold of the solid phase. In a two-dimensional continuum, $c = 1 - p$ and $c_p = 1 - p_c$. We will use the convention that above the percolation threshold refers to states where the liquid phase is continuous.

Restricted diffusion and the size of solid-phase domain units

The diffusion coefficient of a phospholipid decreases as the temperature is decreased (Fig. 6, recall that $D = \omega^2/4\tau$) mainly because of formation of solid-phase domains, which restrict the movement of molecules insoluble in the solid (4, 9, 31, 32). A solid-phase domain of an arbitrary shape can be approximately described by juxtaposition of identical regular geometric units of an appropriate size and shape. We shall refer to those units as solid-phase obstacles and reserve the term solid domain for a connected conglomerate of units.

If the percolation threshold for the liquid phase p_c is low, then the geometric units used can be circular. When

the obstacles are random overlapping circles, p_c = 0.33 (33).

In our previous work (9), we have shown how it is possible to estimate the radius R of solid-phase units or obstacles using a simple model that takes into account the ordering effect of these obstacles on the adjacent liquid phase. This effect decays exponentially away from the obstacle with a coherence length ξ of ~10–20 Å (34–36). Thus, around each obstacle, an annulus of liquid phase that extends a distance δ into the liquid phase exists where the relative diffusion coefficient $D^*(r)$ is smaller than in the bulk liquid phase. Here, r is the radial distance from the obstacle center. As r approaches 0 from above, $D^*(r) \to 0$, and as $r \to \delta$, $D^*(r) \to 1$. Please see Fig. 9 of Almeida et al. (9) for a definition of δ and ξ and for a plot of $D^*(r)$ as a function of r.

The relative average diffusion coefficient in the two-phase system is $\langle D \rangle = D/D_0$, where D is the actual diffusion coefficient in the two-phase system, and D_0 is the diffusion coefficient that would be observed at the same temperature if the system were completely in the liquid phase,

$$\langle D \rangle = 1 - c\left(\frac{R+\delta}{R}\right)^2 + \frac{2c}{R^2}\int_R^{R+\delta} D^*(r) r\, dr + D_{\text{overlap}}. \quad (3)$$

The second term subtracts the area of the obstacles plus annuli, and the third term adds back $\langle D \rangle$ integrated over the annuli; D_{overlap} is a set of correction terms that becomes important only when the solid unit obstacles are very small, $R \simeq \xi$ (9).

This model is now used to interpret the dependence of the diffusion coefficient on the solid area fraction in DMPC/DSPC/cholesterol mixtures. The values of the diffusion coefficient D, obtained from the relation $D = \omega^2/4\tau$, were converted to $\langle D \rangle$ by dividing by D_0; a simple Arrhenius temperature dependence was used for D_0, with an apparent activation energy of 7 kcal/mol as before (9). This is a good approximation for both l_o and l_d phases, though it becomes an underestimation when $l_d - l_o$ transition takes place. We ignore this possible complication. The relative diffusion coefficient $\langle D \rangle$ in mixtures of DMPC/DSPC 1:1 containing cholesterol between 4 and 35 mol% is plotted in Fig. 8 as a function of the solid area fraction. In the mixtures containing 25 and 35 mol% cholesterol, although the diffusion coefficient appears to go to zero, the percolation threshold is never reached (Figs. 6 and 7). This illustrates the importance of determining the recovery as well and not basing the estimation of the percolation threshold on the diffusion coefficient only. The straight line in the upper panel is a fit of Eq. 3 to the data for the mixture containing 15 mol% cholesterol (*filled triangles*); the only variable parameter is R/ξ and a value of 3.6 was obtained, corresponding to a solid obstacle radius of ~40 Å. It is evident that the fit is poor.

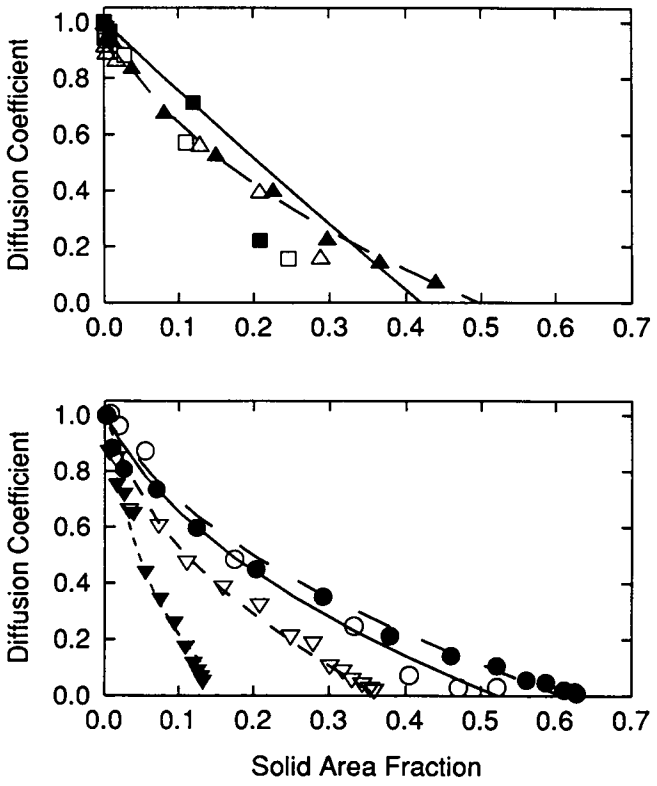

FIGURE 8 Relative diffusion coefficient $\langle D \rangle$ as a function of the solid area fraction in the DMPC/DSPC 1:1 system containing the following cholesterol concentrations (in mol%): *top*, 4 (□), 7 (■), 10 (△), and 15 (▲); *bottom*, 18 (○), 20 (●), 25 (▽), and 35 (▼). The straight line is a fit of Eq. 3 alone to the 15 mol% cholesterol (▲) data. The curves are fits of Eq. 3 and 4 to the data (see text), for the following concentrations of cholesterol (in mol%): *top*, 15 (*dashed line*); *bottom*, 18 (*solid line*), 20 (*long dashes*), 25 (*short dashes*), and 35 (*dotted line*).

A substantial improvement can be made if the radius R is allowed to vary with the solid area fraction c. We have used a linear dependence,

$$R = R_0(1 + kc), \quad (4)$$

where R_0 is the obstacle radius when $c \to 0$ and k is a constant. The analysis depends little on the exact functional form of R. When the approximation of the obstacles by circles is acceptable (when the percolation threshold c_p of the solid phase is not too small, say $c_p \geq 0.5$), it is possible to describe the experimental data using Eqs. 3 and 4. The curves representing the best fits are shown in Fig. 8. The parameter $k = 4$ was the same for all concentrations of cholesterol.

The dependence of the solid obstacle radius on the concentration of cholesterol obtained from the fits is shown in Fig. 9, where R_0 and R at $c = 0.30$ are shown. Variations in the apparent radius between 15 and 20 mol% cholesterol are probably a consequence of a change in the geometry of the obstacles. In this portion of the plot, the average values are $\langle R_0 \rangle = 1.7\xi$ and

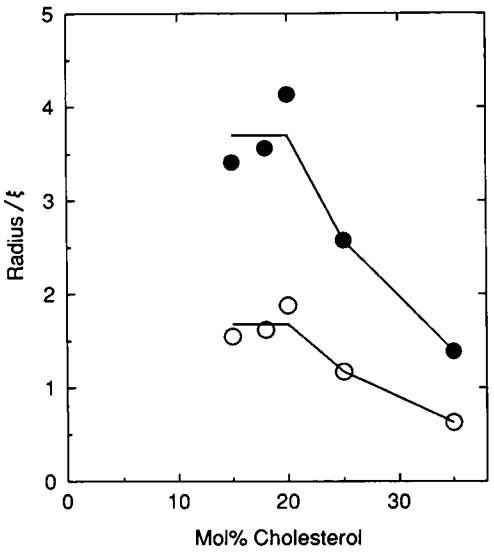

FIGURE 9 Radius R of solid obstacles in units of the coherence length $\xi \simeq 10$–20 Å in DMPC/DSPC/cholesterol as a function of cholesterol concentration. The value in the limit of zero solid fraction R_o (○) and the value of R (●) at 0.30 solid area fraction are shown. The flat line in the initial portion marks the average of the first three points in each plot (values given in the text).

$\langle R \rangle = 3.7\xi$ ($\xi \simeq 15$ Å). Above 20 mol% cholesterol, the solid-phase obstacle radius decreases as the cholesterol concentration increases. Although the exact values of the radius depend on the model, the general trend is model-independent; it is known from Monte Carlo simulations that the smaller the obstacles, the larger the reduction they cause in the diffusion coefficient of a tracer (4, 32).

The solid obstacle radius (Fig. 9) and the enthalpy of the transition (Fig. 5) vary in a parallel manner with the cholesterol concentration. The value of ΔH reflects the difference between the molecular interactions in the solid and liquid phases. High levels of cholesterol reduce ΔH. That is partially due to formation of l_o phase, removing solid phospholipid from the melting transition. However, the decrease in solid domain size beyond 20 mol% cholesterol can probably be explained only if, at these concentrations, cholesterol also decreases the difference between the interactions in the two phases. As the partitioning of cholesterol into the solid is very low, this probably means that cholesterol addition beyond 20 mol% causes an improvement of interactions in the l_o phase. Once the l_o phase is formed, an increase in cholesterol concentration causes an increase in the diffusion activation energy, which reflects the molecular interactions (10). Then, when the interactions in both phases are more similar, the free energy of the interface is lower and the size of the solid-domain units is smaller because the need to minimize the interface length is decreased.

Percolation thresholds and liquid domain sizes

Fig. 10 shows the variation of the limiting fluorescence recovery with the total area fraction of liquid phases (l_o + l_d) in DMPC/DSPC/cholesterol calculated from the data in Fig. 6 and the temperature dependence of the liquid area fractions. In DMPC/DSPC 1:1, the liquid is l_d; in the cholesterol-containing mixtures, it is assumed to be l_o. This assumption appears to be valid for most of the regions of the phase diagram where liquid and solid coexist, as discussed above.

In the absence of cholesterol, the recovery remains high even at low fractions of fluid. Cholesterol decreases fluctuations in lipid bilayers (10). If fluctuations are the reason for this high recovery in DMPC/DSPC 1:1, then we would expect addition of cholesterol to lower the recovery below p_c, in the ternary mixtures, which is observed. The size of the liquid-phase domains located on the circumference of the bleached spot also may play a role, because below p_c larger liquid domains result in a larger recovery. This possibility is consistent with the dependence of the apparent liquid domain size on cholesterol concentration.

To calculate the percolation threshold in each mixture, we further assume that the FRAP fractional recov-

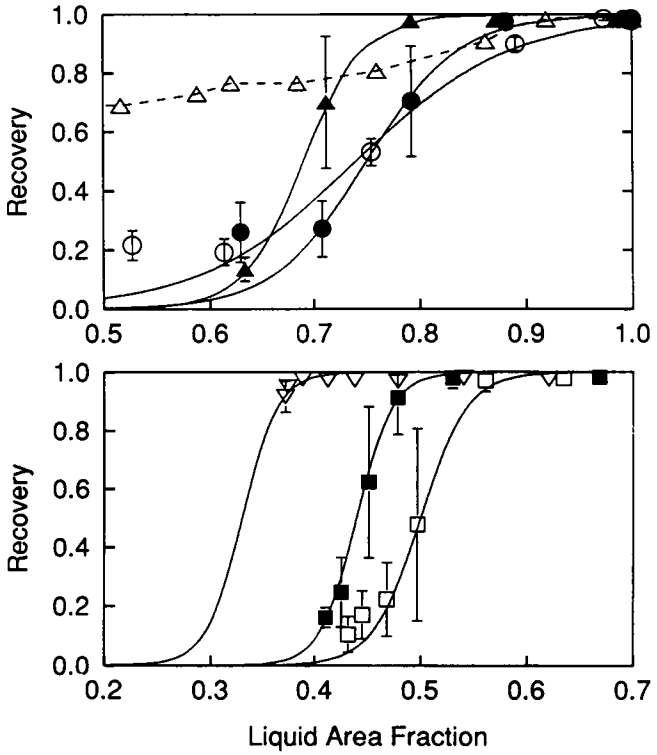

FIGURE 10 Fractional recovery as a function of the liquid area fraction in DMPC/DSPC 1:1 with various concentrations of cholesterol (in mol%): *top*, 0 (△), 4 (○), 7 (●), and 10 (▲); *bottom*, 15 (□), 18 (■), and 20 (▽). Only the region of the threshold is shown. Notice that the horizontal scale is the same but shifted in one panel relative to the other. The lines are fits of Eq. 7 to the data beginning at the first point below p_c in all panels. This excludes the points at smaller area fractions that are clearly out of the curve (see text for reason). The data corresponding to 0 mol% cholesterol, taken from Vaz et al. (6), cannot be fitted by Eq. 7, and the line shown is just to guide the eye.

ery gives the probability of percolation of the liquid phase in each bilayer. This seems a reasonable assumption, if we recall that the systems studied consist of stacks of a few hundred bilayers. At a given fraction of liquid, there is a certain probability that the liquid phase percolates in each bilayer, and the monitored recovery reflects an average over all bilayers.

From finite size scaling in percolation theory (3), it is known that the percolation probability in finite systems depends on the area fraction p of a given phase as

$$R(p) = f[L^{1/\nu}(p - p_c)], \tag{5}$$

where $R(p)$ is the percolation probability, p is the fraction of the phase that reaches the percolation threshold at $p = p_c$, L is the linear dimension of the system (distance between the two ends across which percolation is assessed), and $\nu = 4/3$ is a critical exponent (3). The function f is continuous everywhere and obeys the following conditions,

$$f \to 0 \quad \text{when} \quad p \to 0,$$
$$f \to 1 \quad \text{when} \quad p \to 1.$$

By analogy to a two-state system in thermodynamics, for large L, we can approximate f by

$$f(y) = \frac{\exp(y)}{1 + \exp(y)},$$

with

$$y = AL^{1/\nu}(p - p_c), \tag{6}$$

where $\exp(y)$ is the relative probability that the liquid phase percolates and $1 + \exp(y)$ is the total probability (normalization factor). The constant A can be determined from a fit of this equation to Monte Carlo simulation data, where both L (size of the lattice) and p_c are known. We used for this purpose the data of Saxton (37) and obtained $A = 3.5$. Thus, an explicit expression for the percolation probability of the liquid phase is

$$R(p) = \frac{\exp[AL^{1/\nu}(p - p_c)]}{1 + \exp[AL^{1/\nu}(p - p_c)]}. \tag{7}$$

In Fig. 10, the curves represent the fits of Eq. 7 to the data, allowing both p_c and L to vary. The percolation threshold p_c is the inflection point in the curve and $L^{1/\nu}$ is proportional to the slope of the curve at p_c. It the mixture containing 20 mol% cholesterol, only p_c was fitted; L was obtained from a linear extrapolation of the numbers found for the other concentrations (Fig. 11). The error resulting from identifying $p_{100\%}$ with the percolation threshold is apparent if we compare the curves for 4 and 7 mol% cholesterol; p_c is roughly the same in both but $p_{100\%}$ is not.

The values L and p_c, obtained from the fits, are plotted in Fig. 11 as a function of cholesterol concentration; they

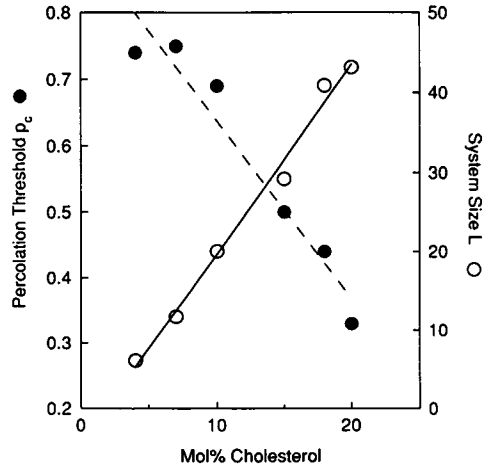

FIGURE 11 Percolation threshold p_c (●, *dashed line*) and system size L (○, *solid line*) in DMPC/DSPC/cholesterol as a function of cholesterol concentration. The system sizes obtained from the fits in Fig. 10 were normalized to the same spot radius of 2.5 μm (individual values of the spot radius varied between 2.49 and 2.64 μm). The lines are simply straight lines through the points.

seem to be inversely correlated, which is not fortuitous as will be apparent shortly. It can be concluded that addition of cholesterol shifts the percolation threshold of the liquid phase to lower area fractions of liquid. If the solid phase is viewed as resulting from a random configuration of overlapping units of elliptical shape with an appropriate size and eccentricity (33), then we may conclude that these units are relatively asymmetric at low cholesterol concentrations (and also, by extrapolation, in DMPC/DSPC 1:1) and become nearly circular at high cholesterol levels.

What does the system size L mean in a lipid two-phase system? In a two-dimensional lattice it is simply the length (in units of lattice distance) between the two ends across which percolation is determined. In continuum percolation, the unit of lattice distance is replaced by the diameter of the circles that constitute the percolating phase (38). It appears to us that the simplest interpretation is to identify the size L as the ratio between the size of the bleached spot and the average size of the finite liquid-phase domain at the percolation threshold in a lipid two-phase system. Here, finite simply means that the percolating ("infinite") cluster, when present, is not taken into the average.

A few problems persist, however. In our FRAP experiments, the bleached spot is circular (as opposed to the square cells used in Monte Carlo simulations), recovery occurs through the entire circumference of the spot, and the liquid domains are not circles; it is therefore impossible to precisely establish the meaning of system size L. We define $L = \omega/\phi$, where ω is the bleached spot radius and ϕ is an average characteristic length of the liquid domains. If the liquid domains were circular, then ϕ

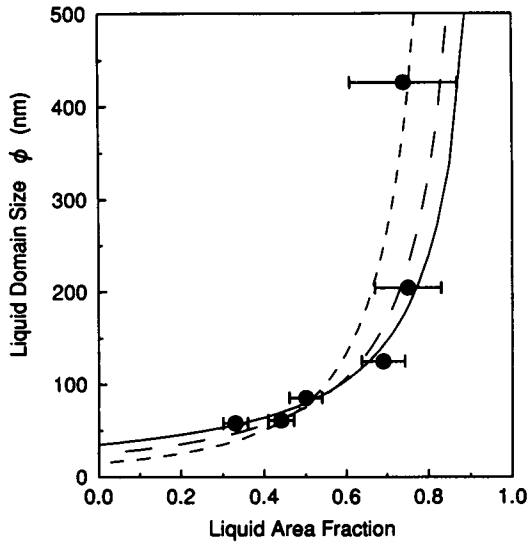

FIGURE 12 Average size of the finite liquid-phase domains in the neighborhood of the percolation threshold as a function of the liquid area fraction at p_c. The curves are calculated from Eq. 11 (see text for details). The error bars are only valid up to a constant factor. For easy reference, the high cholesterol region corresponds to the left side of this plot and the low cholesterol region to the right side.

would probably be roughly equal to their diameter. For the sake of simplicity, we shall refer to ϕ as the domain length. This analysis shows how the liquid domain size can be estimated experimentally by varying ω in a FRAP experiment.

The values of ϕ calculated in this way for each cholesterol concentration are plotted in Fig. 12 as a function of the liquid area fraction at p_c. Strictly speaking, finite size scaling in percolation applies only to large systems. The method may be inappropriate for systems with $L = 6$ (the smallest value we obtained for 4 mol% cholesterol). However, Monte Carlo simulations (38) in the exact range of our values ($L = 5$–40) show that the error in the estimation of the percolation threshold is already small for systems of these sizes.

The uncertainty Δp_c in the determination of p_c increases as the system size L decreases (3),

$$\Delta p_c \sim L^{-1/\nu}. \tag{8}$$

The error bars represented in Fig. 12 are calculated from Eq. 8 with a constant of proportionality of 1/2. This arbitrary value for the constant reflects our estimate of the error. However, although the absolute magnitudes of the error bars are only valid up to a constant factor, their relative magnitudes should be nearly correct, and it is thus possible to have a good idea of the relative error associated with each point.

According to percolation theory, in a infinite system below p_c the average cluster area S of a phase with fractional area p varies as

$$S \sim |p - p_c|^{-\gamma}, \tag{9}$$

where $\gamma = 43/18$ is a critical exponent (3). The cluster size thus becomes infinite at p_c. If the clusters, or domains, are circular, then $\phi \sim S^{1/2}$. If the domains are not compact centrosymmetric structures, then the characteristic length ϕ must depend on the area S according to a more general relation,

$$\phi \sim S^{1/d}, \tag{10}$$

where d is the dimensionality of the domain.

Although the lipid bilayer is finite, we still expect that the average liquid domain size close to the percolation threshold should increase according to a function similar to Eq. 9. On the other hand, statistical mechanical calculations of the cluster size of lipid phases in pure DPPC (39, 40) indicate that the average cluster size of a given phase diverges only when the transition is close to completion and the whole system is in that phase. We thus propose to replace $|p - p_c|^{-\gamma}$ in Eq. 9 by $|p - 1|^{-\gamma}$. This form is, however, not rigorously justified and should be considered hypothetical at this point. With this modification, and substituting S from Eq. 9 into Eq. 10, we obtain

$$\phi = \phi_o |p - 1|^{-\gamma/d}. \tag{11}$$

In Fig. 12, Eq. 11 is compared with the points calculated from the FRAP experimental data. Our hypothetical equation appears to agree with the experimental data quite well. The solid line corresponds to a dimensionality $d = 2$, the long-dashed line to $d = 1.5$, and the short-dashed line to $d = 1$. The average length of the liquid domains in the limit of zero liquid fraction ϕ_o was adjusted to improve the fit. The values of ϕ_o for the curves shown are 35, 25, and 15 nm, for $d = 2$, 1.5, and 1, respectively. It is clear that the worse fit is obtained with $d = 1$, but the data do not allow for an exact determination of the dimensionality; a value between 1.5 and 2 appears to be best.

CONCLUSION

In this ternary system, the dependence of the liquid domain sizes on the liquid area fraction is in good agreement with percolation theory. Addition of cholesterol between 4 and 20 mol% has virtually no effect on the size of the liquid-phase domains if the comparison is made at a constant liquid area fraction. The apparent decrease in liquid domain length ϕ (increase in L; Fig. 11) is completely accounted for by the shift in p_c brought about by cholesterol (Fig. 12). Thus, changing the cholesterol concentration moves the domain length along the line defined by Eq. 11 (Fig. 12); the larger the value of p_c (the larger the area fraction of liquid phase at the percolation threshold), the larger is the observed size of the liquid domains at that point.

In the same interval of cholesterol concentration, the solid-phase unit size is also little affected by varying the cholesterol content. A qualitative interpretation of the change in p_c using continuum percolation arguments (33) suggests that cholesterol causes the solid domain units to become more centrosymmetric. However, the calculated dimensionality of the liquid domains is close to 2 and is not necessarily changed by an increase in cholesterol concentration.

Finally, it is apparent that solid phases can exist at cholesterol concentrations higher than predicted from the behavior of binary mixtures containing cholesterol, because of a differential partitioning of this molecule between the possible phases in more complex mixtures. However, addition of cholesterol shifts the percolation point to higher solid-phase fractions, which decreases the possibility of solid phase acting as a means of disconnecting reactant protein molecules in mammalian plasma membranes. The high levels of cholesterol present in these membranes suggest that a barrier to diffusion of many proteins may be provided by the l_o phase (10). A biologically important control may consist in the switching between the connectivities of l_o and l_d phases.

It is a pleasure to thank Dr. Rodney Biltonen for helpful discussions and for the use of his calorimeter. We also thank Kim Thompson for his expert help with the calorimeter. Finally, we are grateful to Dr. Michael Saxton for his comments, to Dr. Eurico Melo for providing the curve fitting programs, and to Dr. M. B. Sankaram for providing the ESR DMPC/cholesterol and DSPC/cholesterol phase diagrams and for helpful discussions.

This work was supported in part by grants GM-14628 and GM-23573 from the National Institutes of Health, and in part by the Max-Planck-Institut für biophysikalische Chemie, for which we thank Dr. Thomas Jovin.

Received for publication 25 June 1992 and in final form 13 October 1992.

REFERENCES

1. Wu, S. H., and H. M. McConnell. 1975. Phase separations in phospholipid membranes. *Biochemistry.* 14:847–854.
2. Mabrey, S., and J. M. Sturtevant. 1976. Investigation of phase transitions of lipids and lipid mixtures by high sensitivity differential scanning calorimetry. *Proc. Natl. Acad. Sci. USA.* 73:3862–3866.
3. Stauffer, D. 1985. Introduction to Percolation Theory. *Taylor & Francis,* London. 1–24.
4. Saxton, M. J. 1987. Lateral diffusion in an archipelago: the effect of mobile obstacles. *Biophys. J.* 52:989–997.
5. Thompson, T. E., M. B. Sankaram, and R. L. Biltonen. 1992. Biological membrane domains. Functional significance. *Comments Mol. Cell. Biophys.* 8:1–15.
6. Vaz, W. L. C., E. C. C. Melo, and T. E. Thompson. 1989. Translational diffusion and fluid domain connectivity in a two-component, two-phase phospholipid bilayer. *Biophys. J.* 56, 869–876.
7. Vaz, W. L. C., E. C. C. Melo, and T. E. Thompson. 1990. Fluid-phase connectivity in an isomorphous, two-component, two-phase phosphatidylcholine bilayer. *Biophys. J.* 58:273–275.
8. Bultmann, T., W. L. C. Vaz, E. C. C. Melo, R. B. Sisk, and T. E. Thompson. 1991. Fluid-phase connectivity and translational diffusion in a eutectic, two-component, two-phase phosphatidylcholine bilayer. *Biochemistry.* 30:5573–5579.
9. Almeida, P. F. F., W. L. C. Vaz, and T. E. Thompson. 1992. Lateral diffusion and percolation in two-component, two-phase lipid bilayers. Topology of the solid-phase domains in-plane and across the lipid bilayer. *Biochemistry.* 31:7198–7210.
10. Almeida, P. F. F., W. L. C. Vaz, and T. E. Thompson. 1992. Lateral diffusion in the liquid phases of dimyristoylphosphatidylcholine/cholesterol lipid bilayers: a free volume analysis. *Biochemistry.* 31:6739–6747.
11. Ipsen, J. H., G. Karlstroem, O. G. Mouritsen, H. Wennerstroem, and M. J. Zuckermann. 1987. Phase equilibria in the phosphatidylcholine-cholesterol system. *Biochim. Biophys. Acta.* 905: 162–172.
12. Ipsen, J. H., O. G. Mouritsen, and M. J. Zuckermann. 1989. Theory of thermal anomalies in the specific heat of lipid bilayers containing cholesterol. *Biophys. J.* 56:661–667.
13. Shimshick, E. J., and H. M. McConnell. 1973. Lateral phase separations in binary mixtures of cholesterol and phospholipids *Biochem. Biophys. Res. Commun.* 53:446–451.
14. Gordon, P. 1968. Principles of phase diagrams in materials systems. *Krieger,* Malabar, FL. 46–106.
15. Vist, M. R., and J. H. Davis. 1990. Phase equilibria of cholesterol/dipalmitoylphosphatidylcholine mixtures: ^{2}H nuclear magnetic resonance and differential scanning calorimetry. *Biochemistry.* 29:451–464.
16. Sankaram, M. B., and T. E. Thompson. 1990. Interaction of cholesterol with various glycerophospholipids and sphingomyelin. *Biochemistry.* 29:10670–10675.
17. Sankaram, M. B., and T. E. Thompson. 1991. Cholesterol-induced fluid-phase immiscibility in membranes. *Proc. Natl. Acad. Sci. USA.* 88:8686–8690.
18. Sankaram, M. B., and T. E. Thompson. 1990. Modulation of phospholipid acyl chain order by cholesterol. A solid-state ^{2}H nuclear magnetic resonance study. *Biochemistry.* 29:10676–10684.
19. Rubenstein, J. L. R., B. A. Smith, and H. M. McConnell. 1979. Lateral diffusion in binary mixtures of cholesterol and phosphatidylcholines. *Proc. Natl. Acad. Sci. USA.* 76:15–18.
20. Owicki, J. C., and H. M. McConnell. 1980. Lateral diffusion in inhomogeneous membranes: model membranes containing cholesterol. *Biophys. J.* 30:383–398.
21. Snyder, B., and E. Freire. 1980. Compositional domain structure in phosphatidylcholine-cholesterol and sphingomyelin-cholesterol bilayers. *Proc. Natl. Acad. Sci. USA.* 77:4055–4059.
22. Slater, G., and A. Caille. 1982. A percolation model for lateral diffusion in cholesterol-phospholipid mixtures. *Biochim. Biophys. Acta.* 686:249–252.
23. Vaz, W. L. C., and D. Hallmann. 1983. Experimental evidence against the applicability of the Saffman-Delbrueck model to the translational diffusion of lipids in phosphatidylcholine bilayer membranes. *FEBS (Fed. Eur. Biochem. Soc.) Lett.* 152:287–290.
24. Soumpasis, D. M. 1983. Theoretical analysis of fluorescence photobleaching recovery experiments. *Biophys. J.* 41:95–97.
25. Bartlett, G. R. 1959. Phosphorus assay in column chromatography. *J. Biol. Chem.* 234:466–468.
26. Estep, T. N., D. Mountcastle, R. L. Biltonen, and T. E. Thompson. 1978. Studies on the anomalous thermotropic behavior of aqueous dispersions of dipalmitoylphosphatidylcholine-cholesterol mixtures. *Biochemistry.* 17:1984–1989.
27. Wiener, M. C., R. M. Suter, and J. F. Nagle. 1989. Structure of the

fully hydrated gel phase of dipalmitoylphosphatidylcholine. *Biophys. J.* 55:315–325.

28. Demel, R. A., J. W. C. M. Jansen, P. W. M. van Dijck, and L. L. M. van Deenen. 1977. The preferential interactions of cholesterol with different classes of phospholipids. *Biochim. Biophys. Acta.* 465:1–10.
29. Knoll, W., K. Ibel, and E. Sackmann. 1981. Small-angle neutron scattering study of lipid phase diagrams by the contrast variation method. *Biochemistry.* 20:6379–6383.
30. Knoll, W., K. Ibel, G. Schmidt, and E. Sackmann. 1983. Critical demixing in fluid bilayers of phospholipid mixtures: a neutron diffraction study. *J. Chem. Phys.* 79:3439–3442.
31. Saxton, M. J. 1982. Lateral diffusion in an archipelago: effects of impermeable patches on diffusion in a cell membrane. *Biophys. J.* 39:165–173.
32. Saxton, M. J. 1989. Lateral diffusion in an archipelago: distance dependence of the diffusion coefficient. *Biophys. J.* 56:615–622.
33. Xia, W., and Thorpe, M. F. 1988. Percolation properties of random ellipses. *Phys. Rev. A.* 38:2650–2656.
34. Owicki, J. C., M. W. Springgate, and H. M. McConnell. 1978. Theoretical study of protein-lipid interactions in bilayer membranes. *Proc. Natl. Acad. Sci. USA.* 75:1616–1619.
35. Owicki, J. C., and H. M. McConnell. 1979. Theory of protein–protein interactions in bilayer membranes. *Proc. Natl. Acad. Sci. USA.* 76:4750–4754.
36. Jähnig, F. 1981. Critical effects from lipid–protein interactions in membranes. *Biophys. J.* 36:329–345.
37. Saxton, M. J. 1991. Lateral diffusion in an archipelago: shifts in the percolation threshold. *Biophys. J.* 59:627*a*. (Abstr.)
38. Lee, S. B., and S. Torquato. 1990. Monte Carlo study of correlated continuum percolation: universality and percolation thresholds. *Phys. Rev. A* 41:5338–5344.
39. Biltonen, R. L., and E. Freire. 1978. Thermodynamic characterization of conformational states of biological macromolecules using differential scanning calorimetry. *CRC Crit. Rev. Biochem.* 5:85–124.
40. Freire, E., and R. Biltonen. 1978. Estimation of molecular averages and equilibrium fluctuations in lipid bilayer systems from the excess heat capacity function. *Biochim. Biophy. Acta.* 514:54–68.